= 13° and $\varphi'$ = 70°). The activation energy for this barrier is, therefore, 18.0 kcal mol$^{-1}$, which is fairly close to the observed value. The decrease of the potential minimum at $\varphi$ = 100° (−19.6 kcal mol$^{-1}$) is only 6.3 kcal mol$^{-1}$ by the tilting ($\theta$ = −4° and $\varphi'$ = −65°), keeping the potential energy of the second minimum still higher (by 10.1 kcal mol$^{-1}$) than the lowest potential energy. The results suggest a two-site jumping between the unequal potential depths for the molecular motion of **3**. However, this model is not confirmed at present, because the high-temperature region of the $T_{1\rho}$ curve for **3** has not been measured.[20] Thus, the molecular motion for **3** is not fully appreciated yet.

**d. 1,8-Dimethylnaphthalene (4).** The potential energy profile for the in-plane rotation of **4** around the axis through the average position of all the carbon atoms is of much interest. Since the molecule has no $C_2$ axis perpendicular to the molecular plane, the in-plane rotation is not 180° flipping (see Figure 4). Three maxima of the potential energy appear at 155, 236, and 305°, but their values are not so high (−24.2, −24.4, and −26.0 kcal mol$^{-1}$, respectively) compared with the minimum value at 0° (−34.7 kcal mol$^{-1}$). In this energy profile, there are several metastable states with the potential energies higher by ca. 3 kcal mol$^{-1}$ than the most stable state. The reason for observation of no molecular motion for **4** by $T_1$ measurements may be ascribable to its relatively low melting point (337 K) and the expected long $T_1$ minimum. If **9** and **10** have crystal structures similar to the crystal structure of **4** and the potential minima increase for one reason or another, the molecular motion for **9** and **10** is explained by the in-plane molecular reorientation or rotational diffusion among many sites. The latter model was adopted to interpret the temperature dependence of their proton $T_1$ values.[19] We tried to determine the crystal structure of **9** by X-ray crystallography, but unfortunately high-angle reflections were not detected effectively because of rapid molecular motion even at room temperature.

**Acknowledgment.** We thank Professor Eiji Ōsawa of Hokkaido University for his kind offer of the MMPI program source. We also thank Dr. Yoshitaka Beppu of Nagoya University for allowing us to use his program NAMOD in drawing Figures 1–3. The efficient services of the Data Processing Center at Kyoto University and the Computer Center at the Institute for Molecular Science are gratefully acknowledged.

**Registry No. 1**, 2717-39-7; **2**, 91-20-3; **3**, 571-61-9; **4**, 569-41-5.

# Laser–Ion Beam Photodissociation Studies of $C_6H_6^+$ Radical Cations: The 2,4-Hexadiyne System

**R. E. Krailler,[†] D. H. Russell,*[†] M. F. Jarrold,[‡] and M. T. Bowers*[‡]**

*Contribution from the Department of Chemistry, Texas A&M University, College Station, Texas 77843, and the Department of Chemistry, University of California, Santa Barbara, California 93106.* *Received October 15, 1984*

**Abstract:** The results of a laser–ion beam study of the photodissociation of $C_6H_6^+$ ions are presented. In the visible wavelength range of the argon ion laser, $C_6H_6^+$ ions from 2,4-hexadiyne were the only $C_6H_6^+$ ions for which photodissociation was observed. The observed products were $C_6H_5^+$, $C_6H_4^+$, $C_4H_4^+$, and $C_3H_3^+$. The absorption was assigned to a $\tilde{A}^2E_u \leftarrow \tilde{X}^2E_g$ transition in the 2,4-hexadiyne cation. The photodissociation spectrum, photofragment branching ratios, information on the product relative kinetic energies, and photofragment angular distributions are presented and discussed along with the results of statistical theory model calculations. We conclude that dissociation of 2,4-hexadiyne cation $\tilde{A}^2E_u$ proceeds by internal conversion to the ground state followed by vibrational predissociation. The relatively large anisotropy of the photofragment angular distributions indicates that isomerization to a benzene structure does not precede dissociation.

## I. Introduction

The benzene ion and other $C_6H_6^+$ radical cations have been studied since the earliest days[1] of mass spectrometry and gas-phase ion chemistry. One motivation for this interest is that the benzene ion is one of the simplest hydrocarbon ions, so understanding this system is important from a fundamental point of view. The size of the research effort directed toward understanding the $C_6H_6^+$ system is demonstrated by a recent review[2] devoted entirely to this problem.

In recent years two key issues have emerged. First, for nondissociating $C_6H_6^+$ ions, which of the possible structural isomers are stable and what are the barriers to isomerization? Second, for $C_6H_6^+$ ions with sufficient internal energy to dissociate, does relaxation from excited states to the ground state and/or isomerization precede dissociation?

Determining the structures of gas-phase ions has always been difficult. The application of conventional spectroscopic techniques is usually not possible owing to the low ion densities. In addition, the low-energy requirements for hydrogen and carbon skeleton rearrangements make structural assignment of hydrocarbon ions particularly challenging. Collision-induced dissociation (CID), probably the most widely used technique for probing ion structures, does not generally yield distinguishable "fingerprint" spectra for hydrocarbon ions.[3] For $C_6H_6^+$ CID is of little utility since the CID spectra of $C_6H_6^+$ isomers (benzene and acyclic) are very similar.[4] Bimolecular reactivity studies[5] have identified three distinct cyclic $C_6H_6^+$ isomers—benzene, fulvene (5-methylene-1,3-cyclopentadiene), and 3,4-dimethylenecyclobutene—which are distinguishable from the linear isomers 1,3-hexadien-5-yne, 1,5-hexadiyne, and 2,4-hexadiyne. However, the linear isomers of $C_6H_6^+$ could not be differentiated. Which of the ground-state linear isomers of $C_6H_6^+$ are stable (i.e., have a minimum on the

[†] Texas A&M University.
[‡] University of California, Santa Barbara.

(1) See, for example: Momigny, J.; Brakier, L.; D'or, L. *Bull. Cl. Sci., Acad. R. Belg.* **1962**, *48*, 1002. Rosenstock, H. M.; Krauss, M. *Adv. Mass Spectrom.* **1962**, *2*, 251.
(2) Rosenstock, H. M.; Dannacher, J.; Liebman, J. F. *Radiat. Phys. Chem.* **1982**, *20*, 7.
(3) See, for example: Wagner-Redeker, W.; Illies, A. J.; Kemper, P. R.; Bowers, M. T. *J. Am. Chem. Soc.* **1983**, *105*, 5719.
(4) Borchers, F.; Levsen, K. *Org. Mass Spectrom.* **1975**, *10*, 584.
(5) Gross, M. L.; Russell, D. H.; Aerni, R. J.; Bronczyk, S. A. *J. Am. Chem. Soc.* **1977**, *99*, 3603. Russell, D. H.; Gross, M. L. *J. Am. Chem. Soc.* **1980**, *102*, 6279.

0002-7863/85/1507-2346$01.50/0 

potential energy surface) is not known.

Unraveling the behavior of $C_6H_6^+$ ions with sufficient internal energy to dissociate is more difficult than probing stable $C_6H_6^+$ ions. The debate over the role of isolated electronic states and noncommunicating isomeric structures in the dissociation of $C_6H_6^+$ ions has been going on for over a decade.[6] To date, perhaps the most direct and definitive information comes from photoion–photoelectron coincidence (PIPECO) studies. Baer and co-workers[7] have performed PIPECO measurements of the dissociation rates of $C_6H_6^+$ ions derived from benzene, 2,4-hexadiyne, and 1,5-hexadiyne. Placing the data on a common total energy scale, they concluded that benzene, 2,4-hexadiyne, and 1,5-hexadiyne ions with the same total energy in the range 14.8–15.6 eV dissociate at the same rate. They interpreted this result as indicating that these $C_6H_6^+$ ions rapidly interconvert prior to dissociation. However, the argument presented by Baer and co-workers is not as watertight as it first appears. There is some uncertainty about the heats of formation of the neutral species, and to get the rates to match, the heat of formation of 2,4-hexadiyne must be lowered by 0.18 eV. Furthermore, there appear to be conflicting results concerning the behavior of 2,4-hexadiyne ions formed in the $\tilde{A}^2E_u$ first excited electronic state. Baer and co-workers[7] interpreted their PIPECO results as indicating that dissociation from the $\tilde{A}^2E_u$ state proceeds by internal conversion followed by dissociation on the ground-state surface. However, the PIPECO results of Dannacher and co-workers[8,9] are not consistent with this interpretation but instead suggest either that dissociation occurs directly from the $\tilde{A}^2E_u$ excited electronic state or that isomerization does not occur on the ground-state surface.

In this paper we report the results of a study of the photodissociation of the 2,4-hexadiyne cation and other $C_6H_6^+$ ions. Measurements were performed by using the ion beam/laser beam instruments at Texas A&M University (TAMU) and the University of California, Santa Barbara (UCSB). In addition to the experimental data, we present the results of some statistical theory model calculations for the 2,4-hexadiyne system. The data reported here are relevant to both issues discussed above: the structure of stable $C_6H_6^+$ ions and understanding the detailed mechanism of dissociation of excited $C_6H_6^+$ ions. From a broader perspective, the results presented here are relevant to the recent multiphoton ionization (MPI) studies of benzene and other $C_6H_6$ molecules.[10] The mechanism of extensive fragmentation of the various $C_6H_6$ isomers on MPI is poorly understood.[11] Information obtained under single-photon excitation conditions may help to unravel the MPI fragmentation process.

The rest of this paper is organized as follows. In the next section (Experimental Section) we describe the experimental apparatuses at TAMU and UCSB. Then in the Results we present the experimental results. This is followed by a Discussion in which the data are discussed along with the results of statistical theory model calculations. The paper ends with brief Conclusions and an Appendix.

## II. Experimental Section

The experimental work described in this paper was performed at Texas A&M University (TAMU) and the University of California, Santa Barbara (UCSB). The experimental apparatus at TAMU, shown

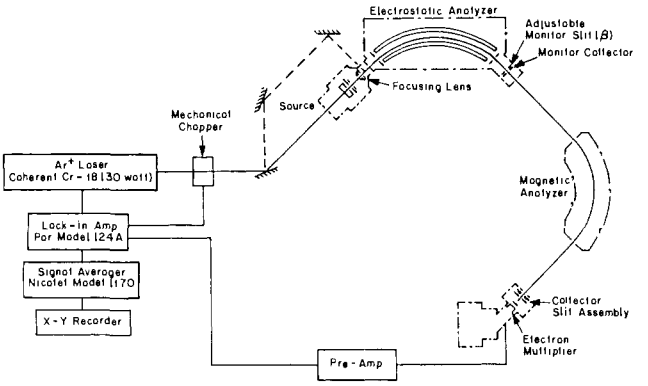


**Figure 1.** Schematic diagram of the laser–ion beam photodissociation apparatus at Texas A&M University.

schematically in Figure 1, consists of a Kratos (AEI) MS-902 double-focusing mass spectrometer, a Coherent CR-18 argon ion laser, and the necessary electronic components for laser modulation and data acquisition. The mass spectrometer is equipped with a programmable high-voltage power supply (Wallis Model R103/3), a digital waveform generator (Wavetek Model 159) for high-voltage programming, and an adjustable energy-resolving slit ($\beta$-slit). The accelerating potential is monitored by a Keithley 4 1/2 digit multimeter. The laser beam is aligned coaxially with the ion beam by using mirrors with micrometer adjustment for fine control. Laser alignment is accomplished by adjusting the mirrors to achieve a maximum photodissociation signal for loss of H from 2,4-hexadiyne. The laser beam enters the ion source housing through a sapphire window mounted on the source flange, passes through the ion source repeller (1 × 3 mm slit), and enters the first field-free region. In addition, perpendicular laser–ion beam experiments can be performed by admitting the laser beam into the first field-free region through a sapphire window mounted on the analyzer housing. For maximum sensitivity the majority of the experiments were performed with a coaxial laser–ion beam configuration. However, critial data were remeasured by using a perpendicular laser–ion beam configuration. No significant difference between the two experimental configurations was observed.

Photofragment ions formed in the first field-free region are transmitted through the electrostatic analyzer by scanning the accelerating voltage over a small range centered about $V \times m_2/m_1$ (where $m_1$ is the mass of the reactant ion, $m_2$ is the mass of the fragment ion, and $V$ is the voltage required to focus the main beam). Unimolecular "metastable" dissociation and collision-induced dissociation yield a signal more than 10 times larger than the photofragment ion signal. The photofragment signal is detected by mechanically chopping the laser beam and measuring the difference between the "laser on" and "laser off" signals. The difference signal is obtained with a lock-in amplifier (PAR Model 124A). To enhance the signal-to-noise ratio, the signal is accumulated and averaged by using a Nicolet 1170 signal averager. The high-voltage scanning and signal-averaging systems are slaved to the waveform generator.

The experimental apparatus at UCSB has been described in detail elsewhere[12,13] so will only be briefly reviewed here. The experiment consists of a reverse-geometry mass spectrometer (VG Instruments, ZAB-2F) and an argon ion laser (Coherent Innova 20). Ions extracted from the source are accelerated to 8 kV and mass analyzed by the magnet. The mass-selected ion beam is then crossed with the laser beam in the second field-free region, and the photofragments are analyzed by the electrostatic analyzer. The UCSB experiment, with a crossed-beam configuration, is less sensitive than the TAMU experiment. However, the UCSB experiment is better suited to measuring photoproduct kinetic energy distributions and can also provide information on the photoproduct angular distributions.

Discrimination against product ions with a large velocity component perpendicular to the ion beam direction is a problem with the instrumental configurations employed in these experiments. However, for the data reported here no significant errors are expected because the product relative kinetic energies are relatively small.

The experiments were performed under low-pressure electron impact conditions. All reagents were obtained from commercial sources:

(6) See, for example, Andlauer, B.; Ottinger, Ch. *J. Chem. Phys.* **1971**, *55*, 1471. Andlauer, B.; Ottinger, Ch. *Z. Naturforsch. A* **1972**, *27*, 293. Rosenstock, H. M.; Larkins, J. T.; Walker, J. A. *Int. J. Mass Spectrom. Ion Phys.* **1973**, *11*, 309. Chupka, W. A. In "Chemical Spectroscopy and Photochemistry in the Vacuum–Ultraviolet"; Sandorfy, C.; Ausloos, P. J.; Robin, M. B., Eds.; Reidel: Dordrecht, 1974, p 433. Beynon, J. H.; Caprioli, R. M.; Perry, W. O.; Baitinger, W. E. *J. Am. Chem. Soc.* **1972**, *94*, 6828.

(7) Baer, T.; Willet, G. D.; Smith, D.; Phillips, J. S. *J. Chem. Phys.* **1979**, *70*, 4076.

(8) Dannacher, J. *Chem. Phys.* **1978**, *29*, 339.

(9) Dannacher, J.; Stadelmann, J.-P.; Vogt, J. *J. Chem. Phys.* **1981**, *74*, 2094.

(10) See, for example: Zandee, L.; Bernstein, R. B. *J. Chem. Phys.* **1979**, *70*, 2574. Boesl, U.; Neusser, H. J.; Schlag, E. W. *J. Chem. Phys.* **1980**, *72*, 4327. Gobeli, D. A.; Morgan, J. R.; St. Pierre, R. J.; El-Sayed, M. A. *J. Phys. Chem.* **1984**, *88*, 178.

(11) Schlag, E. W.; Neusser, H. J. *Acc. Chem. Res.* **1983**, *16*, 355. Rebentrost, F.; Ben-Shaul, A. *J. Chem. Phys.* **1981**, *74*, 3255.

(12) Jarrold, M. F.; Illies, A. J.; Bowers, M. T. *J. Chem. Phys.* **1983**, *79*, 6086.

(13) Jarrold, M. F.; Illies, A. J.; Bowers, M. T. *J. Chem. Phys.* **1984**, *81*, 214.

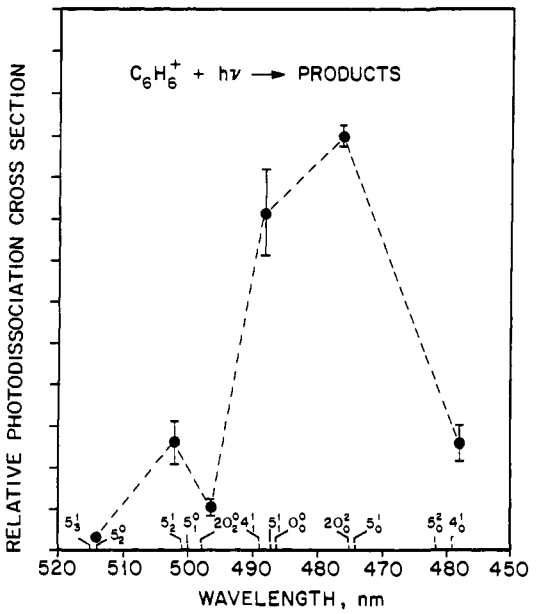


Figure 2. Photodissociation spectrum of the $C_6H_6^+$ ions from 2,4-hexadiyne. The points are the average of three experimental measurements. The error bars shown are ±1 standard deviation. The dashed line joining the points is a guide to give an indication of the shape of the absorption profile. The vibronic transitions on the wavelength axis were taken from ref 23. The experimental conditions were ionizing electron energy = 70 eV and ion source temperature = 450 K.

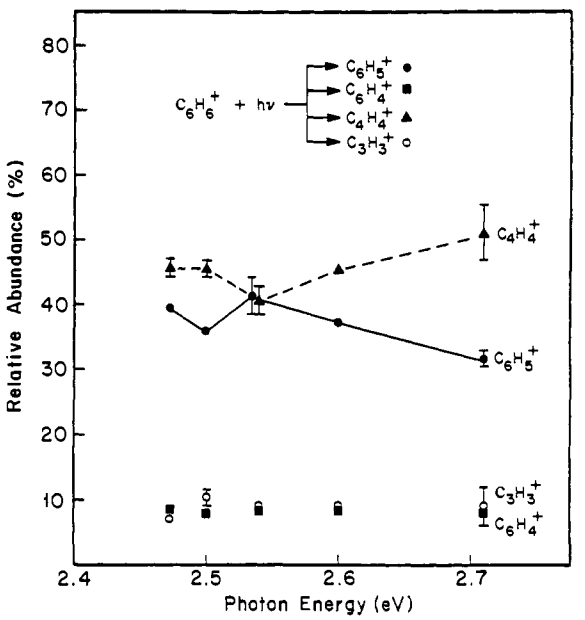


Figure 3. Product branching ratios for the photodissociation of $C_6H_6^+$ ions from 2,4-hexadiyne. The points are the average of four experimental measurements. The error bars show ±1 standard deviation. Lines are drawn between some of the data points to make the figure clearer. The experimental conditions were ionizing electron energy = 70 eV and ion source temperature = 450 K.

benzene, styrene, benzaldehyde, and anisole were obtained from MCB, 2,4-hexadiyne and 1,5-hexadiyne were obtained from Pfaltz & Bauer, and 2,4,6-cycloheptatrienone was obtained from Alpha. The samples were purified by several freeze–pump–thaw cycles to remove any noncondensable gases.

## III. Results

As part of this work we have investigated the visible wavelength photodissociation of a relatively large number of $C_6H_6^+$ ions, e.g., benzene, 2,4-hexadiyne, 1,5-hexadiyne, and $C_6H_6^+$ from 2,4,6-cycloheptatrienone, benzaldehyde, anisole, and styrene. In the visible wavelength range of the argon ion laser (514–455 nm) the only precursor that produces photofragmenting $C_6H_6^+$ is 2,4-hexadiyne. On the basis of comparative measurements, we estimate the photofragment signal for the other $C_6H_6^+$ isomers is less than 1% that of 2,4-hexadiyne $C_6H_6^+$.

The photodissociation reactions observed for 2,4-hexadiyne $C_6H_6^+$ ions were loss of H, $H_2$, $C_2H_2$, and $C_3H_3$:

$$C_6H_6^+ + h\nu \rightarrow C_6H_5^+ + H \quad (1)$$

$$\rightarrow C_6H_4^+ + H_2 \quad (2)$$

$$\rightarrow C_4H_4^+ + C_2H_2 \quad (3)$$

$$\rightarrow C_3H_3^+ + C_3H_3 \quad (4)$$

Studies of the laser power dependence of the photofragment signals indicate that the observed photodissociation arises from a single-photon process.

**A. Photodissociation Spectrum.** The photodissociation spectrum measured on the TAMU instrument was derived in the following manner. The photofragment intensities for each product ion were obtained from the photofragment peak areas. The intensities were then corrected for the variation of the reactant ion density in the first field-free region as described in section IIIB. Finally, the individual intensities were summed together and divided by the photon flux. The result is a relative total photodissociation cross section, which is plotted as a function of wavelength in Figure 2.

The photodissociation spectrum shown in Figure 2 is clearly bimodal. There is a small maximum around 502 nm, a minimum around 497 nm, and a large maximum near 480 nm.

**B. Photodissociation Product Branching Ratios.** The photodissociation product branching ratios measured on the TAMU instrument are displayed in Figure 3. The branching ratios were derived from photofragment intensities taken from the photofragment peak areas. In the TAMU experiment the photofragment ions are detected by adjusting the accelerating voltage so that the products are transmitted through the electrostatic analyzer (ESA) with a nominal energy of approximately 4 kV. Thus the ion flux in the interaction region changes with the product monitored. The total ion current (measured between the ESA and the magnet) and the reactant ion current (measured at the detector) varied by less than 15% over the accelerating voltage range required to focus all the products. The data shown in Figure 3 have not been corrected for this small change in ion current. Although the ion current remains essentially constant over the accelerating voltage range used, the ion density in the laser–ion beam interaction region changes because the reactant ions' velocity varies with the accelerating voltage. To correct for this variation the photofragment intensities were multiplied by $(m_1/m_2)^{1/2}$ (where $m_1$ is the mass of the reactant ion and $m_2$ is the mass of the product ion). The corrected individual photofragment intensities were then summed and the product branching ratios calculated as a percentage of the total photofragment intensity.

$C_4H_4^+$, with a relative abundance of approximately 45%, is the dominant ion at all wavelengths, followed closely by $C_6H_5^+$, with a relative abundance of approximately 35%. As the photon energy is increased to 2.71 eV (458 nm) the relative abundance of $C_4H_4^+$ increases to 51% while the $C_6H_5^+$ ion intensity drops off to 32%. The decrease of $C_4H_4^+$ relative abundance at 488 nm may be real, although the scatter in the data is fairly large. The relative abundances of $C_6H_4^+$ and $C_3H_3^+$ are nearly constant across the wavelength range studied and are both less than 10%.

**C. Photofragment Angular Distributions.** Photodissociation products are not in general distributed isotropically.[14] Photon absorption arises from the interaction of the transition dipole moment of the ion with the electric vector of the laser beam. Ions with their transition dipole moments aligned with the laser beam electric vector have a higher probability for photoexcitation. This results in an excited ion population with an anisotropic distribution

(14) Zare, R. N.; Herschbach, D. R. *Proc. IEEE* **1963**, *51*, 173. Zare, R. N. *Mol. Photochem.* **1972**, *4*, 1.

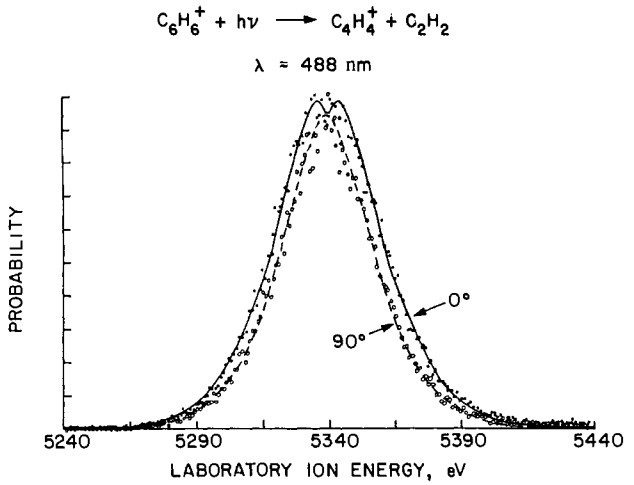


**Figure 4.** Peak shapes measured for the $C_4H_4^+$ product from the photodissociation of $C_6H_6^+$ (2,4-hexadiyne) at 488 nm. Peak shapes are shown for the laser beam polarization at 0° and 90° with respect to the ion beam direction. The points are the experimental data and the lines are a theoretical fit using a velocity-dependent asymmetry parameter (see text). The experimental conditions were energy resolving power = 2700 (fwhm), ionizing electron energy = 20 eV, and ion source temperature = 320 K.

of molecular orientations which will be reflected in the product angular distributions. The photofragment angular distribution has the general form[14,15]

$$P(\theta) = (4\pi)^{-1}[1 + \beta P_2(\cos\theta)] \quad (5)$$

where $P(\theta)$ is the probability, per unit solid angle, that the products recoil at an angle $\theta$ with respect to the electric vector, $P_2(\cos\theta)$ is the second-degree Legendre polynomial in $\cos\theta$, and $\beta$ is the asymmetry parameter. The asymmetry parameter can have values between +2 and −1 and reflects the degree of anisotropy of the product angular distributions: values of $\beta$ equal to +2 or −1 represent maximum possible anisotropy, and $\beta$ equal to zero indicates an isotropic distribution. The degree of anisotropy of the product angular distributions depends on a number of factors including the detailed dynamics of dissociation and the lifetime of the excited ion. If the excited ion survives for several rotational periods the anisotropy will be substantially reduced but the angular distributions will not in general be isotropic.[16,17]

Information on the photoproduct angular distributions was obtained by using the UCSB laser–ion beam experiment. This experiment has a crossed-beam configuration, and the orientation of the laser beam polarization with respect to the ion beam direction can be changed with a polarization rotator. Since the electrostatic analyzer measures essentially the energy along the ion beam direction, if the angular distribution is anisotropic, the photofragment peak shapes measured with the laser polarization at different orientations with respect to the ion beam direction will be different. Photofragment peak shapes measured for $C_4H_4^+$ at 488 nm with the laser beam polarization at 0° and 90° are shown in Figure 4 The peak shapes are slightly different, which indicates that the photofragment angular distributions are slightly anisotropic. Similar results were obtained for the $C_3H_3^+$ photofragment. We were not able to record any reliable data for the $C_6H_5^+$ and $C_6H_4^+$ photofragments, or for the $C_4H_4^+$ and $C_3H_3^+$ photofragments at wavelengths other than 488 nm, because of the lower sensitivity of the crossed-beam configuration and the large unimolecular "metastable" background.

It is possible to analyze the 0° and 90° peak shapes shown in Figure 4 to derive more quantitative information about the product angular distributions. The procedures used to analyze the peak shapes have been described in detail elsewhere.[18] Briefly, the

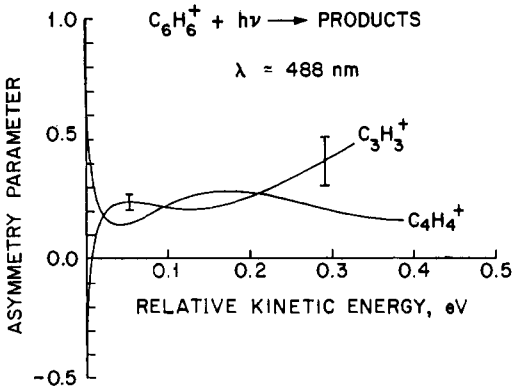


**Figure 5.** Plot of the asymmetry parameter against product relative kinetic energy for $C_4H_4^+$ and $C_3H_3^+$ from the photodissociation of $C_6H_6^+$ (2,4-hexadiyne) at 488 nm. The data were derived by using a fifth-order polynomial expansion of the asymmetry parameter and a least-squares fit to the 0° and 90° peak shapes as described in the text.

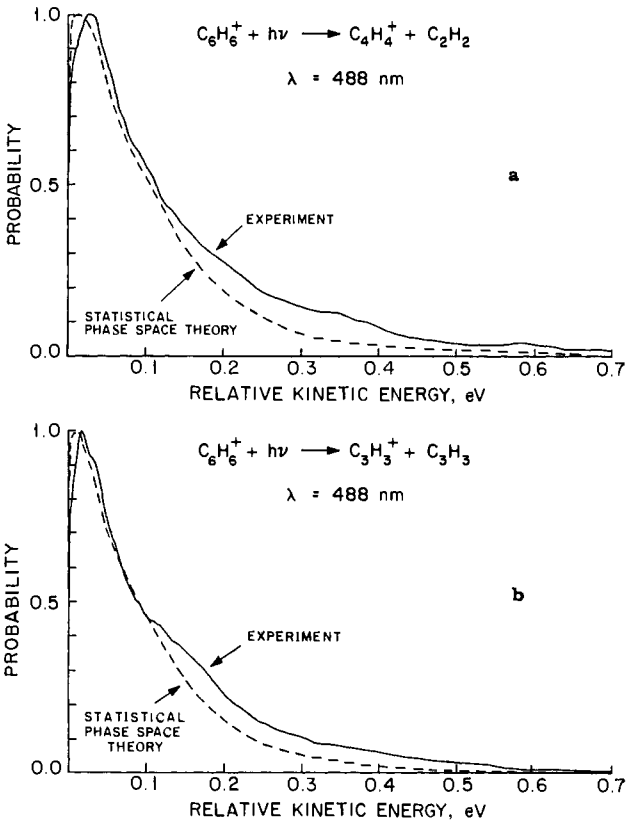


**Figure 6.** Photofragment relative kinetic energy distributions for (a) $C_4H_4^+$ and (b) $C_3H_3^+$ from photodissocation of $C_6H_6^+$ (2,4-hexadiyne) on the UCSB instrument. The solid lines are the experimental results and the dashed lines are the results of statistical phase space theory calculations (see text). The experimental conditions were energy resolving power = 2700 ($C_4H_4^+$) and 2000 ($C_3H_3^+$), ionizing electron energy = 20 eV, and ion source temperature = 320 K.

product relative velocity distribution is convoluted, with the photofragment angular distribution given by eq 5. The asymmetry parameter $\beta$ is represented by a polynomial:

$$\beta = \beta_0 + \beta_1 u + \beta_2 u^2 + \ldots \quad (6)$$

where $u$ is the product relative velocity. A least-squares procedure is used to determine the coefficients in eq 6 by fitting calculated peak shapes to the measured 0° and 90° peak shapes. The results of this analysis are shown in Figures 4 and 5. In Figure 4 the least-squares-fit peak shapes for $C_4H_4^+$, calculated by using a

(15) Busch, G. E.; Wilson, K. R. *J. Chem. Phys.* **1972**, *56*, 3638.
(16) Jonah, C. *J. Chem. Phys.* **1971**, *55*, 1915.
(17) Yang, S.; Bersohn, R. *J. Chem. Phys.* **1974**, *61*, 4400.
(18) Jarrold, M. F.; Illies, A. J.; Bowers, M. T. *J. Chem. Phys.*, in press.

fifth-order polynomial for $\beta$, are compared with the experimental data. The values of the asymmetry parameter for the $C_4H_4^+$ and $C_3H_3^+$ products, derived with fifth-order polynomials, are plotted in Figure 5 against the product relative kinetic energy.

The values of the asymmetry parameter plotted in Figure 5 are not very reliable for the larger values of relative kinetic energy because the product intensity at large kinetic energies is small (see the product relative kinetic energy distributions shown in Figure 6). For kinetic energies up to 0.25 eV the asymmetry parameters for both the $C_4H_4^+$ and the $C_3H_3^+$ products are fairly similar, with values around 0.2. A least-squares analysis of the 0° and 90° peak shapes, assuming that $\beta$ does not change with the product relative kinetic energy, yields most probable values for the asymmetry parameter of 0.20 for $C_4H_4^+$ and 0.23 for $C_3H_3^+$.

**D. Photofragment Relative Kinetic Energies.** Photofragment relative kinetic energy distributions were measured for $C_4H_4^+$ and $C_3H_3^+$ products at 488 nm on the UCSB instrument. Reliable data could not be measured for $C_6H_5^+$ and $C_6H_4^+$, or for $C_4H_4^+$ and $C_3H_3^+$ at other wavelength owing to the large unimolecular "metastable" background and the low sensitivity of the crossed-beam configuration.

The product relative kinetic energy distributions are obtained from the photofragment peak shapes. As we have discussed above, the photofragments are not scattered isotropically and the peak shapes vary with the orientation of the laser beam polarization with respect to the ion beam direction. We have shown elsewhere[13] that with the laser polarization at the "magic angle" of 54.7° with respect to the ion beam direction, the peak shape is identical with that which would be obtained if the photofragments were distributed isotropically. This "magic angle" peak can be analyzed in the same straightforward way as unimolecular "metastable" peaks to obtain the product relative kinetic energy distribution. The transformation from a peak shape to a relative kinetic energy distribution is accomplished by numerically differentiating the peak shape and transforming the energy axis to the center-of-mass frame.[19]

The photofragment relative kinetic energy distributions measured at 488 nm are shown in Figure 6. The distribution for the $C_4H_4^+$ product peaks near 0.03 eV, and then the probability falls off slowly, approaching zero at >0.6 eV. The shape of the $C_3H_3^+$ product distribution is very similar to the $C_4H_4^+$ distribution, though slightly narrower. The $C_3H_3^+$ product distribution peaks at ~0.02 eV and approaches zero at ~0.6 eV. Product relative kinetic energy distributions were also measured for the unimolecular "metastable" dissociation. For both $C_4H_4^+$ and $C_3H_3^+$ the product relative kinetic energy distributions for unimolecular "metastable" dissociation were slighty narrower than the distributions for photodissociation.

Further information on the product relative kinetic energies was derived from measurements at TAMU. These measurements were performed as a function of wavelength for all four reaction channels: $C_6H_5^+$, $C_6H_4^+$, $C_4H_4^+$, and $C_3H_3^+$. The information about the product relative kinetic energies was obtained from the full width at half-maximum (fwhm) of the photofragment peaks and corrected for the main-beam contribution to the peak width by using the expression[20]

$$T = \frac{m_2 \text{ eV}}{16 m_1 m_3}\left(\frac{\Delta v_{m^*} - \Delta V_{mb}}{V}\right)^2 \qquad (7)$$

In eq 7, $V$ is the main-beam accelerating voltage, $\Delta V_{m^*}$ is the fwhm of the product peak, $\Delta V_{mb}$ is the fwhm of the main-beam peak, and $m_1$, $m_2$, and $m_3$ are the masses of the reactant ion, product ion, and product neutral, respectively. For a Gaussian peak shape the product relative kinetic energies obtained from eq 7 correspond to the most probable kinetic energy,[20] if the angular distribution

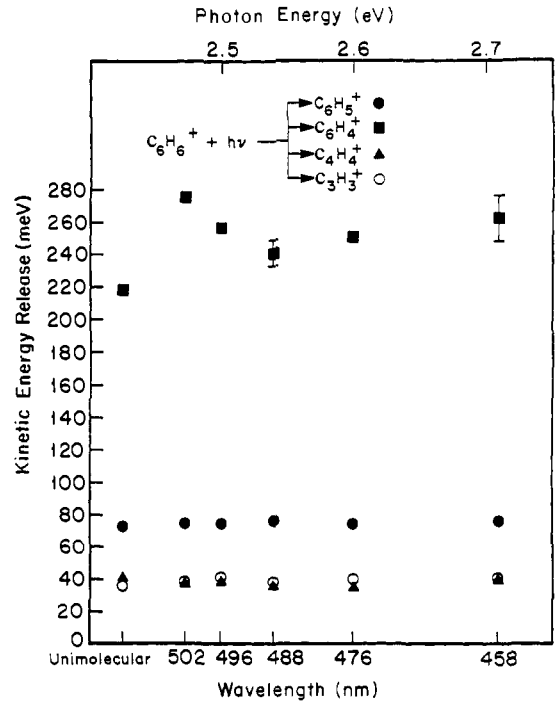


Figure 7. Photofragment relative kinetic energies derived from the fwhm of the photofragment peaks measured at TAMU. Data are shown for $C_6H_5^+$ (●), $C_6H_4^+$ (■), $C_4H_4^+$ (▲), and $C_3H_3^+$ (○) products measured over the wavelength range 502–458 nm and also for unimolecular "metastable" dissociation in the first field-free region. The experimental conditions were energy resolving power = 1000, ionizing electron energy = 70 eV, and ion source temperature = 450 K.

is isotropic. With the coaxial laser–ion beam configuration the laser beam polarization is perpendicular to the ion beam direction, and so the measured peaks correspond to the 90° peaks recorded at UCSB. Since the 0° and 90° peak shapes (Figure 4) are not very different, substantial uncertainty will not be introduced by the anisotropy of the product angular distributions, and the kinetic energies derived by using eq 7 will roughly correspond to the most probable values.

The data are displayed in Figure 7. For $C_6H_5^+$, $C_4H_4^+$, and $C_3H_3^+$ the product kinetic energies are essentially constant over the wavelength range studied, with values of approximately 75, 40, and 40 meV, respectively. For these three product channels the product kinetic energy for unimolecular "metastable" dissociation is very close to the photofragment values. The data for $C_4H_4^+$ and $C_3H_3^+$ are in qualitative agreement with the UCSB data. For the $H_2$-loss channel the photofragment kinetic energies are much larger than those of the other three channels, with values around 260 meV. The kinetic energies change slightly with wavelength, with an apparent minimum at 488 nm. The uncertainty associated with the $H_2$-loss data is quite large because the photofragment signal for this channel is very weak and the background "metastable" signal is large. However, the variation shown in Figure 7 was reproducible. For the $H_2$-loss channel the product kinetic energy for unimolecular "metastable" dissociation is significantly smaller than the photofragment kinetic energies.

## IV. Discussion

The photoelectron spectrum of 2,4-hexadiyne[21] shows that the first excited $\tilde{A}^2E_u$ state lies at an energy around 2.56 eV above the $\tilde{X}^2E_g$ ground state. The 2,4-hexadiyne cation is one of the few large ions that are known to fluoresce and $\tilde{X}^2E_g \leftarrow \tilde{A}^2E_u$ emission has been studied on several occasions.[22,23] The transition

(19) Jarrold, M. F.; Illies, A. J.; Kirchner, N. J.; Bowers, M. T.; Mandich, M. L.; Beauchamp, J. L. *J. Phys. Chem.* **1983**, *87*, 2213 and references therein.

(20) Cooks, R. G.; Beynon, J. H.; Caprioli, R. M.; Lester, G. R. "Metastable Ions"; Elsevier: New York, 1973.

(21) Brogli, F.; Heilbronner, E.; Hornung, V.; Kloster-Jensen, E. *Helv. Chim. Acta* **1973**, *56*, 2171. Bieri, G.; Burger, F.; Heilbronner, E.; Maier, J. P. *Helv. Chim. Acta* **1977**, *60*, 2213.

(22) Allan, M.; Maier, J. P.; Marthaler, O.; Kloster-Jensen, E. *Chem. Phys.* **1978**, *29*, 331.

**Table I.** Comparison of the Photofragment Branching Ratios with PIPECO Branching Ratios and the Results of Statistical Theory Models

| | | PIPECO[b] | | stat theory[a] | |
|---|---|---|---|---|---|
| product | photodissoc[a] | ref 7 | ref 8 | cyclic[c] | linear[b] |
| $C_6H_5^+$ | 39 | 57 | 76 | 45 | 31 |
| $C_6H_4^+$ | 9 | 16 | 16 | 12 | 5 |
| $C_4H_4^+$ | 44 | 20 | 8 | 30 | 45 |
| $C_3H_3^+$ | 9 | 7 | <1[e] | 12 | 18 |

[a] Averaged over the wavelength range 476–514 nm. [b] PIPECO branching ratio at approximately the same total energy as the photodissociation results. [c] Assuming a phenyl structure for $C_6H_5^+$ and a benzyne structure for $C_6H_4^+$. [d] Assuming linear structures for $C_6H_5^+$ and $C_6H_4^+$. [e] Not observed.

responsible for the photodissociation process observed in the present work is almost certainly $\tilde{A}^2E_u \leftarrow \tilde{X}^2E_g$. The $\tilde{A}^2E_u$ excited state is known from $\tilde{X}^2E_g \leftarrow \tilde{A}^2E_u$ emission studies[22] to have a long lifetime (24 ± 2 ns). However, on the time scale of our experiments the $\tilde{A}^2E_u$ state and other excited electronic states will have decayed before reaching the laser–ion beam interaction region so that only ground-state ions will be available for photoexcitation. It is known from the emission studies[22] and PIPECO studies[8] that emission from the $\tilde{A}^2E_u$ state is in competition with nonradiative decay. Ultimately the nonradiative decay channel gives rise to the products we observe in these photodissociation studies.

We have shown on the photodissociation spectrum (Figure 2) the location of a number of vibronic transitions taken from the $\tilde{X}^2E_g \leftarrow \tilde{A}^2E_u$ emission spectrum. The transitions were taken from a high-resolution study[23] in a supersonic jet (temperature ~30 K). At the ion source temperature at which our measurements were performed (450 K) the closely spaced levels would not be resolved and there would be considerable overlap between the more widely separated groups of levels.

It is evident from Figure 2 that all the argon ion laser lines with which measurements were performed lie close to a cluster of vibronic transitions. The 488-nm line lies close to the $4_1^1$, $5_1^1$, and $0_0^0$vibronic transitions. These are transitions in which there is no change in vibrational state. The 502-nm line lies close to vibronic transitions with $\Delta v_5 = -1$ (i.e., $5_2^1$ and $5_1^0$:vibronic transitions in which the $v_5$ mode changes by −1), the 514-nm line is close to $\Delta v_5 = -2$, the 476-nm line is close to $\Delta v_5 = +1$, and the 458-nm line is close to $\Delta v_5 = +2$ and $\Delta v_4 = +1$. The small maximum on the left of the spectrum, therefore, arises from vibrationally excited ground electronic state ions. That this maximum at ~500 nm is small supports predictions from the photoelectron spectrum[21] that the 2,4-hexadiyne ions will be present predominantly in the ground vibrational state of the $\tilde{X}^2E_g$ state.

The largest photodissociation cross section is observed with the 476-nm line. From the photoelectron spectrum[21] and the emission spectrum[22] we would expect the largest photodissociation cross section to be at the 0–0 transition ($\Delta v = 0$), which is close to 488 nm. That the maximum occurs at 476 nm rather than 488 nm may be related to the suggestion of Baer and co-workers[7] that the fluorescence quantum yield is considerably smaller (<20%) in the higher vibrational states than from the $v = 0$ state (60%). If the fluorescence quantum yield is smaller, then the nonradiative decay channel must be larger, and we would therefore expect to see a larger photodissociation cross section.

In Table I the photofragment branching ratios are compared with the PIPECO product branching ratios. The photofragment branching ratios shown in Table I are an average over the wavelength range 514–476 nm. As can be seen from Figure 3, the photofragment branching ratios appear reasonably constant over this wavelength range. The PIPECO data, shown in Table I, were taken from the work of Baer et al.[7] and Dannacher[8] and are for a total energy close to the threshold for the $\tilde{A}^2E_u$ state, which corresponds to the energy regime sampled in our photodissociation experiments. There is rather poor agreement between the two PIPECO data sets. The most significant discrepancy is that Dannacher did not observe any $C_3H_3^+$. Since the experiment of Baer and co-workers is a threshold photoelectron PIPECO experiment, Dannacher and co-workers suggested that the $C_3H_3^+$ observed by Baer et al. could be formed by an autoionization phenomenon. However, we observe $C_3H_3^+$ from photodissociation of 2,4-hexadiyne ions and therefore conclude that $C_3H_3^+$ is one of the products of 2,4-hexadiyne ions excited into the $\tilde{A}^2E_u$ state. We have no explanation for why Dannacher did not observe $C_3H_3^+$ from the 2,4-hexadiyne cation $\tilde{A}^2E_u$ state.

From Table I it can be seen that there is qualitative agreement between the PIPECO branching ratios of Baer et al.[7] and the photofragment branching ratios. Direct comparison between the photofragment and PIPECO branching ratios cannot be made because the photodissociation experiment samples a broader range of internal energies. PIPECO branching ratio measurements indicate that the probability of forming $C_4H_4^+$ product increases with energy in this energy regime. This fact probably accounts for why the photofragment $C_4H_4^+$ relative abundance is substantially larger in the PIPECO measurements and why the $C_4H_4^+$ relative abundance increases at 458 nm (see Figure 3) in our photodissociation studies.

The photofragment relative kinetic energy distributions shown in Figure 6 peak at small values of kinetic energy, and the probability falls off roughly exponentially with increasing kinetic energy. This form of product relative kinetic energy distribution is characteristic of statistical energy disposal. To determine if the energy disposal is statistical we have used statistical phase space theory to calculate product relative kinetic energy distributions for comparison with the experimental data. From the statistical phase space theory the probability that products, with available energy $E$ and total angular momentum $J$, recoil with relative kinetic energy $E_t$ is given by[24]

$$P(E,J;E_t) = \frac{\int dE_r\, \rho_v(E - E_t - E_r) \int dL \int dJ_r\, \rho_r(L_r,J_r)}{\int dE_{tr}\, \rho_v(E - E_{tr})\Gamma_{tr}(E_{tr},J)} \quad (8)$$

in which $\rho$ is a density of states, $\Gamma$ is a sum of states, and the subscripts v, t, and r correspond to vibration, translation, and rotation, respectively. For comparison with the experimental data $P(E,J;E_t)$ must be averaged over the experimental energy and angular momentum distributions:

$$P_i(E_t) = \frac{\int dE\, P(E') \int dJ\, P(J) P_i(E',J) P(E,J;E_t)}{\int dE\, P(E') \int dJ\, P(J) P_i(E',J)} \quad (9)$$

In eq 9, $P_i(E_t)$ is the probability of relative kinetic energy $E_t$ in product channel $i$, $P(J)$ is the angular momentum distribution which is assumed to be given by the thermal distribution of 2,4-hexadiyne, and $P(E')$ is the energy distribution of the photoexcited ions. The photoexcitation process was modeled by assuming that photon absorption moved all energetically accessible ions in the ground state up to the first excited state with equal probability. The energy distribution of the ground-state ions was assumed to be given by the photoelectron spectrum.[8] The emission spectrum[22] shows that $\tilde{X}^2E_g \leftarrow \tilde{A}^2E_u$ emission will not significantly change the energy distribution of the ground-state ions predicted from the photoelectron spectrum. $P_i(E',J)$ in eq 9 is the probability of forming product $i$ at energy $E'$ above the zero-point energy of 2,4-hexadiyne $C_6H_6^+$ and is given by

$$P_i(E',J) = F_i(E',J) / \sum F_i(E',J) \quad (10)$$

where $F_i(E',J)$ is the flux through the tight transition state for product channel $i$ and $\sum F_i(E',J)$ is the total reactive flux obtained by summing over all channels.

The calculations reported in this paper are similar to the statistical theory calculations we have reported for benzene $C_6H_6^+$[25]

(23) Klapstein, D.; Leutwyler, S.; Maier, J. P. *Chem. Phys. Lett.* **1981**, *84*, 534.

(24) Chesnavich, W. J.; Bowers, M. T. *J. Am. Chem. Soc.* **1976**, *98*, 8301. Chesnavich, W. J.; Bowers, M. T. In "Gas Phase Ion Chemistry"; Bowers, M. T., Ed.; Academic Press: New York, 1979; Vol. 1.

and other hydrocarbon ions[26] and so they are not described in great detail here. The selection of the input parameters is described in the Appendix. Some of the input parameters were taken from our earlier work on benzene $C_6H_6^+$.[25] The breakdown graphs obtained from PIPECO studies for benzene and 2,4-hexadiyne are similar, within the limited accuracy of the experimental data, in the energy range relevant to these photodissociation experiments.[7] As before,[25] we have assumed that the $C_4H_4^+$ ion is formed as two structural isomers: a cyclic isomer (methylenecyclopropene) and a linear isomer (vinylacetylene). However, in the energy range relevant to the photodissociation experiments the higher energy linear isomer contributed only around 10% of the calculated $C_4H_4^+$ relative abundance. $C_3H_3^+$ and $C_3H_3$ were assumed to have the structures of the lowest energy isomers: cyclopropenium cation and propargyl radical. As is described in more detail below, calculations were run by using both cyclic and linear isomers for $C_6H_5^+$ and $C_6H_4^+$. The kinetic energy distributions calculated for the $C_4H_4^+$ and $C_3H_3^+$ photofragments were essentially independent of the assumed structure for the $C_6H_5^+$ and $C_6H_4^+$ products.

The results of the calculations are shown in Figure 6, where the calculated relative kinetic energy distributions (dashed lines) are compared with the measured distributions (solid lines) for $C_4H_4^+$ and $C_3H_3^+$. As can be seen from Figure 6 there is good agreement between the calculated and measured distributions for both $C_4H_4^+$ and $C_3H_3^+$. The model appears to underestimate the probabilities at relatively large kinetic energies. This may indiate that the photofragmenting ions contain more internal energy than in the model. We did not include in the model the suggestion of Baer and co-workers[7] that the higher vibrational levels of the $\tilde{A}^2E_u$ state have a lower fluorescence quantum yield (i.e., more dissociation) than the ground vibrational state. This would increase the average energy of the photofragmenting ions.

Calculations were also performed for $C_6H_5^+$, $C_4H_4^+$, and $C_3H_3^+$ products as a function of wavelength. For $C_6H_5^+$ (both linear and cyclic) the calculated distribution has its maximum at significantly larger relative kinetic energies than $C_4H_4^+$ and $C_3H_3^+$. This is consistent with the experimental data shown in Figure 7 (the kinetic energies obtained from the fwhm of the photofragment peaks are larger for $C_6H_5^+$ than for $C_4H_4^+$ and $C_3H_3^+$) and is probably a consequence of the low polarizability of the H atom and angular momentum restrictions. The average kinetic energies calculated from the statistical model for all three channels increased by approximately 10% over the wavelength range studied. This small change is close to the limit that we could reasonably expect to detect from the precision of the data shown in Figure 7. Kinetic energy distributions were not calculated for the $C_6H_4^+$ channel because the large relative kinetic energies observed for this product (see Figure 7) suggest that a reverse activation barrier is present.

The good agreement between the measured photofragment relative kinetic energy distributions and the results of the statistical phase space theory calculations indicates that energy is disposed statistically in the $C_4H_4^+$ and $C_3H_3^+$ product channels. These results confirm the suggestion of Baer and co-workers[7] that dissociation from the $\tilde{A}^2E_u$ state proceeds by internal conversion to the ground state followed by vibrational predissociation (i.e., statistical unimolecular reaction) on the ground-state surface. Direct dissociation from the $\tilde{A}^2E_u$ state would involve electronic predissiciation via a repulsive surface, which would result in nonstatistical energy disposal.

We will now discuss the information we can derive from the product angular distributions. 2,4-Hexadiyne has $D_{3d}$ nuclear symmetry. However, for discussion of the ground and first excited states the electronic symmetry is effectively $D_{\infty h}$ and the electronic transition can be considered as $\tilde{A}^2\Pi_u \leftarrow \tilde{X}^2\Pi_g$.[22] This is a parallel-type transition; there is no change in electronic orbital angular momentum; and the transition dipole moment lies along the carbon skeleton. Parallel-type transitions are expected to result in positive values for the asymmetry parameter, and negative values are expected for perpendicular transitions.[14] Positive values for the asymmetry parameters were derived from the analysis of the 0° and 90° peak shapes, which is consistent with the assignment of the transition to $\tilde{A}^2E_u \leftarrow \tilde{X}^2E_g$.

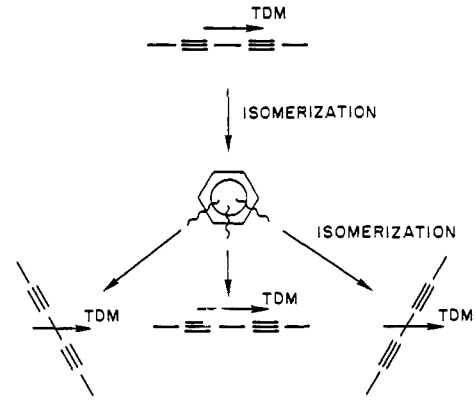


**Figure 8.** Diagram illustrating how isomerization of 2,4-hexadiyne $C_6H_6^+$ to a benzene structure will scramble the internal coordinate system (TDM = transition dipole moment).

For a pure parallel transition the asymmetry parameter can have a maximum allowed value of +2. Several factors reduce the asymmetry parameter from this maximum value. The most important factors are the lifetime of the photoexcited ion and the detailed dynamics of dissociation. If the lifetime of the excited ion is longer than several rotational periods, rotational averaging occurs and the asymmetry parameter is reduced. The reduction in the asymmetry parameter depends on the shape of the ion (i.e., oblate or prolate top).[17] Using the tabulated results of Yang and Bersohn,[17] complete rotational averaging for 2,4-hexadiyne will reduce the asymmetry parameter by a factor of 0.18. Thus for 2,4-hexadiyne values of the asymmetry parameter that lie outside the range $+0.36 > \beta > -0.18$ indicate that complete rotational averaging has not occurred. Values within this range are consistent with complete rotational averaging.

The most probable values for the asymmetry parameters obtained from the analysis of the 0° and 90° peak shapes were 0.20 for $C_4H_4^+$ and 0.23 for $C_3H_3^+$. These values lie within the range expected for complete rotational averaging. A lifetime longer than several rotational periods for 2,4-hexadiyne ion excited into the $\tilde{A}^2E_u$ state is expected from the earlier $\tilde{X}^2E_g \leftarrow \tilde{A}^2E_u$ emission studies[22] where a lifetime in the nanosecond range was deduced.

The asymmetry parameters derived here (0.20 for $C_4H_4^+$ and 0.23 for $C_3H_3^+$) are smaller than the maximum asymmetry parameter expected with complete rotational averaging of 2,4-hexadiyne (0.36). Asymmetry parameters generally do not equal their theoretical maximum values. In the present case, the most likely reason why the measured asymmetry parameter is smaller than the maximum rotationally averaged value is that the products do not all recoil along the direction of the transition dipole moment, which is along the axis of the carbon skeleton of 2,4-hexadiyne. We have previously analyzed the photofragment angular distributions resulting from a statistical unimolecular dissociation.[18] The products recoil at a broad distribution of angles with respect to the axis of the breaking bond because of the distribution of product orbital angular momenta. This results in a reduction in the asymmetry parameter. That the measured asymmetry parameters are only around 60% of the maximum rotationally averaged value is not therefore surprising. What is much more significant, however, is that the asymmetry parameters are as large as 60% of the maximum rotationally averaged value.

If the 2,4-hexadiyne isomerized to a benzene structure before dissociating, the asymmetry parameter would not be expected to be as large as we observe. Isomerization will scramble the internal coordinate system as illustrated in Figure 8. If 2,4-hexadiyne $C_6H_6^+$ sampled a benzene structure before dissociating from a

(25) Jarrold, M. F.; Wagner-Redeker, W.; Illies, A. J.; Kirchner, N. J.; Bowers, M. T. *Int. J. Mass Spectrom. Ion Processes* **1984**, *58*, 63.

(26) Chesnavich, W. J.; Bass, L.; Su, T.; Bowers, M. T. *J. Chem. Phys.* **1981**, *74*, 2228. Jarrold, M. F.; Bass, L. M.; Kemper, P. R.; van Koppen, P. A. M.; Bowers, M. T. *J. Chem. Phys.* **1983**, *78*, 3756.

2,4-hexadiyne structure or other linear structures, the asymmetry parameter would be reduced by an additional factor of 0.25, resulting in a maximum value for the rotationally averaged asymmetry parameter of 0.09.[27] Sampling other cyclic structures such as the fulvene structure and the subsequent effects of the dynamics of dissociation would reduce the asymmetry parameter even further. The relatively large rotationally averaged asymmetry parameters observed here are, therefore, not consistent with isomerization to a cyclic structure.[28] This conclusion conflicts with the conclusions of Baer and co-workers from PIPECO studies.[7] Their conclusions were based on the fact that the dissociation rates from different neutral precursors were the same. However, this is a requirement for, but not proof of isomerization preceding dissociation. Furthermore, as noted in the Introduction, there is uncertainty concerning the heat of formation of neutral 2,4-hexadiyne, so the dissociation rates from different neutral precursors may not in fact be the same.

For total energies around 1 eV above the total energies in the photodissociation experiments there is evidence from the breakdown graphs measured with different precursors that direct dissociation competes with isomerization to a common structure. However, at the total energies in the photodissociation experiments, Baer and co-workers[7] concluded that the relative abundances of the different fragments from benzene and 2,4-hexadiyne are similar within the limited precision of the experimental data. The lowest energy structures for $C_6H_5^+$ and $C_6H_4^+$ are phenyl and benzyne, respectively.[2] It is easy to see how these cyclic products are formed from benzene $C_6H_6^+$. It is difficult to envisage how they could be formed from 2,4-hexadiyne without invoking isomerization to a benzene $C_6H_6^+$ structure. This leads us to postulate that in the energy range of the photodissociation experiments the $C_6H_5^+$ and $C_6H_4^+$ products are mainly higher energy linear structures. To determine if this hypothesis is reasonable some statistical theory calculations of the photofragment product branching ratios were performed. From statistical theory the relative abundance of photofragment $i$ is

$$R_i = \int dE' P(E') \int dJ P(J) \frac{F_i(E',J)}{\sum F_i(E',J)} \qquad (11)$$

in which all the symbols have been defined above. The results of the calculations are shown in Table I. In the column labeled "cyclic" the $C_6H_5^+$ and $C_6H_4^+$ products are assumed to have cyclic structures, and we have used the same input parameters as in our earlier calculations on the $C_6H_6^+$ benzene system.[25] In the column labeled linear we have substituted linear structures for $C_6H_5^+$ and $C_6H_4^+$ in the calculations. There is reasonable agreement between the measured branching ratios and the statistical calculations assuming both linear and cyclic $C_6H_5^+$ and $C_6H_4^+$ products. Fine tuning of the transition-state parameters to achieve better agreement between experiment and theory was not performed for either the linear or cyclic models (see Appendix). These results demonstrate that formation of linear $C_6H_5^+$ and $C_6H_4^+$ from 2,4-hexadiyne in the energy range of the photodissociation experiments is feasible. The higher energy linear structures can compete with the cyclic structures in this energy range because the linear structures are much looser with several low-frequency vibrational modes associated with distortion of the carbon skeleton.

Table II. Input Parameters for the Parent 2,4-Hexadiyne Ion and the Transition States

| param | 2,4-hexadiyne ion | *l*-$C_6H_5^+$ + H tight | *l*-$C_6H_4^+$ + $H_2$ tight | *l*-$C_6H_5^+$ + H orbiting |
|---|---|---|---|---|
| $\nu^a$ | 2953 (2) | 3315 | 3315 (2) | 3315 |
| | 2947 (3) | 2945 | 2938 | 2945 |
| | 2914 | 2938 | 2923 | 2938 |
| | 2265 | 2923 | 2125 | 2923 |
| | 2163 | 2921 | 2116 | 2921 |
| | 1472 (2) | 2125 | 1470 | 2125 |
| | 1428 (2) | 2116 | 1191 | 2116 |
| | 1381 | 1435 | 1188 | 1435 |
| | 1379 | 1434 | 1021 | 1434 |
| | 1030 (2) | 1345 | 962 | 1345 |
| | 1027 (2) | 1337 | 950 | 1337 |
| | 941 | 1191 | 794 | 1191 |
| | 495 | 1188 | 790 | 1188 |
| | 475 (2) | 1021 | 720 (2) | 1021 |
| | 353 (2) | 962 | 670 (2) | 962 |
| | 246 (2) | 950 | 651 (2) | 950 |
| | 228 | 930 | 637 (2) | 930 |
| | 101 (2) | 794 | 489 | 794 |
| | | 637 (2) | 482 | 637 (2) |
| | | 489 | 350 | 489 |
| | | 482 | 322 | 482 |
| | | 350 | 219 | 350 |
| | | 322 | 150 | 322 |
| | | 320 (2) | 134 | 219 |
| | | 219 | | 134 |
| | | 134 | | 89 |
| | | 89 | | |
| $\Delta H_{f^\circ_0}{}^b$ | 13.007 | 14.622 | 14.723 | 14.622 |
| $E_0{}^c$ | | 1.615 | 1.706 | 1.615 |
| $B^d$ | 0.146 | 0.120 | 0.090 | 0.160 |
| $B_{ir}{}^e$ | 2.450 | | | |
| $\sigma^f$ | 6 | 1 | 1 | 1 |
| $\mu^g$ | | | | 0.987 |
| $\alpha^h$ | | | | 0.667 |

[a] Vibrational frequencies in $cm^{-1}$. [b] Heat of formation at 0 K in eV. [c] Zero-point energy difference between 2,4-hexadiyne ion and the transition state in eV. [d] Rotational constant in $cm^{-1}$. [e] Internal rotor rotational constant in $cm^{-1}$. [f] Rotational symmetry number. [g] Reduced mass in amu. [h] Polarizability in $Å^3$.

One piece of data remains to be explained. From the work of Baer and co-workers[7] the total rates of dissociation of $C_6H_6^+$ ions derived from benzene and 2,4-hexadiyne are certainly close if they are not identical. Since 2,4-hexadiyne $C_6H_6^+$ is substantially less stable than benzene $C_6H_6^+$, dissociation from the 2,4-hexadiyne structure would be expected to be much more rapid. The difference in stabilities is partly compensated for by the looser structure of 2,4-hexadiyne. However, total dissociation rates calculated with statistical theory for 2,4-hexadiyne $C_6H_6^+$ are around an order of magnitude larger than the rates calculated with the benzene structure. There are many possible linear structures for $C_6H_6^+$, some of which are more stable than 2,4-hexadiyne.[2] If isomerization to the other linear structures preceded dissociation, the rate would be lower than that calculated on the basis of the 2,4-hexadiyne $C_6H_6^+$ structure alone. Isomerization to other linear structures could easily be achieved by a series of facile hydrogen shifts and would be consistent with our data on the anisotropy of the product angular distributions since isomerization to other linear structures would not scramble the internal coordinate system. Finally we should mention that Dannacher[8] has reported total dissociation rates of $>10^7$ $s^{-1}$ for 2,4-hexadiyne ions excited into the $\tilde{A}^2E_u$ state, which conflicts with the results of Baer and co-workers.[7]

## V. Conclusions

In this paper we have presented the results of a laser–ion beam study of the photodissociation of 2,4-hexadiyne $C_6H_6^+$ ions and $C_6H_6^+$ ions derived from a number of different sources. 2,4-Hexadiyne $C_6H_6^+$ ions were the only $C_6H_6^+$ ions for which

(27) From Figure 8, isomerization through the benzene structure results in three equivalent configurations for 2,4-hexadiyne with the transition dipole moment at 0° and ±60° with respect to the carbon skeleton. The reduction in the value of the asymmetry parameter is given by

$$\frac{1}{3}[P_2(\cos 0°) + 2P_2(\cos 60°)] = 0.25.$$

Combining this with the reduction due to rotational averaging yields $0.36 \times 0.25 = 0.09$.

(28) We should mention a possible alternative explanation for why the measured asymmetry parameters are so large. There may be a small direct (i.e., transition to a repulsive surface) photodissociation component present with a large asymmetry parameter. However, there is no evidence of a direct component in the product relative kinetic energy distributions, the asymmetry parameters remain reasonably constant with product relative kinetic energy, and it seems unlikely that a small direct component should be present for both $C_4H_4^+$ and $C_3H_3^+$ products in roughly the same proportions. We, therefore, consider this possibility as extremely unlikely.

photodissociation was observed. These results, and subsequent analysis, indicate that ground-state 2,4-hexadiyne $C_6H_6^+$ represents a minimum on the $C_6H_6^+$ potential energy surface and does not isomerize to other structures.

Comparison of the photofragment relative kinetic energy distributions with the results of statistical phase space theory calculations indicates that energy is disposed statistically in the $C_4H_4^+$ and $C_3H_3^+$ product channels. This result indicates that 2,4-hexadiyne cations excited into the $\tilde{A}^2E_u$ state dissociate by internal conversion to the ground state followed by vibrational predissociation on the ground-state surface.

PIPECO measurements[7] indicate that the product branching ratios and total dissociation rates for $C_6H_6^+$ ions derived from benzene and 2,4-hexadiyne precursors are similar in the total energy range of the photodissociation experiments. This result was interpreted as indicating that benzene and 2,4-hexadiyne isomerize to a common set of structures before dissociating. However, the relatively large anisotropy of the photoproduct angular distributions reported here indicates that 2,4-hexadiyne $C_6H_6^+$ does not isomerize to a benzene structure before dissociation.

Statistical theory model calculations demonstrated the feasibility of forming higher energy linear $C_6H_5^+$ and $C_6H_4^+$ isomers from the dissociation of 2,4-hexadiyne cations in roughly the same proportions as cyclic isomers are formed from the dissociation of benzene $C_6H_6^+$. This accounts for the similarities between the PIPECO product branching ratios for benzene and 2,4-hexadiyne in the total energy range of the photodissociation experiments. However, total dissociation rates calculated from statistical theory for a 2,4-hexadiyne $C_6H_6^+$ precursor are around an order of magnitude larger than from a benzene $C_6H_6^+$ precursor. We suggest that the dissociation rate of 2,4-hexadiyne $C_6H_6^+$ may be lowered by isomerization to other linear isomers (i.e., it samples a common linear isomer phase space) before dissociation. There is not good agreement on the absolute rate of dissociation of 2,4-hexadiyne $C_6H_6^+$, however, and dissociation of 2,4-hexadiyne ions excited to the $\tilde{A}^2E_u$ state may in fact be faster than dissociation of benzene $C_6H_6^+$ ions of the same energy.

**Acknowledgment.** The work at TAMU was supported by the U.S. Department of Energy, Office of Basic Energy Sciences, and the Robert A. Welch Foundation. Some of the TAMU Equipment was purchased from funds provided by the TAMU Center for Energy and Mineral Resources. The work at UCSB was supported by grants from the National Science Foundation (CHE80-20464) and the Air Force Office of Scientific Research (AFOSR-82-0035).

## Appendix

There are 13 species involved in the calculations reported here: 2,4-hexadiyne parent $C_6H_6^+$ ion, two sets of tight and orbiting transition states for $C_6H_5^+/H$ (a cyclic $C_6H_5^+$ ion and a linear $C_6H_5^+$ ion), two sets of tight and orbiting transition states for $C_4H_4^+/C_2H_2$ (one for a cyclic $C_4H_4^+$ ion and the other for a linear $C_4H_4^+$ ion), and tight and orbiting transition states for $C_3H_3^+/C_3H_3$. For each of these we require an activation energy, rotational constant(s), and vibrational frequencies.

The input parameters for cyclic $C_6H_5^+/H$, cyclic $C_6H_4^+/H_2$, cyclic and linear $C_4H_4^+/C_2H_2$, and $C_3H_3^+/C_3H_3$ were taken directly from the work of Bowers and co-workers.[25]

The heats of formation for the remaining ions were obtained from other sources: 2,4-hexadiyne ion,[2] linear $C_6H_5^+$ ions,[29,30] and linear $C_6H_4^+$ ion.[31] The activation energies for the linear $C_6H_5^+$ transition states were set equal to the zero-point energy difference. The tight transition state for the $C_6H_4^+$ ions was set above the zero-point energy difference (because the large product kinetic energies suggest a reverse activation barrier) and treated as an adjustable parameter.

The vibrational frequencies for 2,4-hexadiyne $C_6H_6^+$ were taken from the neutral.[32] For the $C_6H_5^+$ channel, the values were estimated from neutral 1,5-hexadiyne[33] since a 1,5-hexadiyne like $C_6H_5^+$ is presumably more stable.[29,30] For the orbiting transition state, a triple-bond C–H stretch and two triple-bond C–H bends are deleted. For the tight transition state, the stretch was removed as the reaction coordinate and the two bends were reduced by half. For the $C_6H_4^+$ ion with an assumed 3-hexene-1,5-diyne structure (which is the most stable nonbranched linear isomer),[31] frequencies for the tight transition state were also estimated from 1,5-hexadiyne neutral frequencies.[33] Four $CH_2$ bends and two CH stretches were reduced by half. In addition, the torsion and stretch frequencies associated with the C–C single bond which becomes a C–C double bond were taken as averages of the single- and double-bond values.

Rotational constants were calculated by using typical bond lengths and bond angles. For the tight transition states the rotational constants were calculated averages of assumed geometries at a normal bond length and with a 5-Å bond length.

**Registry No.** 2,4-Hexadiyne radical cation, 61369-13-9; 2,4-hexadiyne, 2809-69-0; 1,5-hexadiyne, 628-16-0; benzene, 71-43-2; styrene, 100-42-5; benzaldehyde, 100-52-7; anisole, 100-66-3; 2,4,6-cycloheptatrienone, 539-80-0.

(29) Dill, J. P.; Schleyer, P. v. R.; Binkley, J.; Seeger, R.; Pople, J. A.; Haselbach, E. *J. Am. Chem. Soc.* **1976**, *98*, 5428.
(30) Tasaka, M.; Ogata, M.; Ichikawa, H. *J. Am. Chem. Soc.* **1981**, *103*, 1885.
(31) Rosenstock, H. M.; Stockbauer, R.; Parr, A. C. *J. Chim. Phys. Phys.-Chim. Biol.* **1980**, *77*, 745.
(32) Ferigle, S. M.; Cleveland, F. F.; Meister, A. G. *J. Chem. Phys.* **1952**, *20*, 1928.
(33) Powell, D. L.; Klaeboe, P.; Phonanatha, A.; Cyvin, B. N.; Cyvin, S. J.; Hopf, H. *J. Mol. Struct.* **1977**, *41*, 203.